RSC Advances

PAPER

View Article Online
View Journal | View Issue



Cite this: *RSC Adv.*, 2023, **13**, 22538

# $Fe_3O_4$ supported [Cu(II)(met)(pro-H)$_2$] complex as a novel nanomagnetic catalytic system for room temperature C–O coupling reactions†

Ahmed Talal Ali,[a] Muthik A. Guda,[b] Amjad I. Oraibi,[c] Issam K. Salih,[d] A. H. Shather,[e] Abbas Talib Abd Ali,[f] Ahmed L. Azzawi[g] and Haider Abdulkareem Almashhadani *[h]

Received 25th May 2023
Accepted 20th July 2023

DOI: 10.1039/d3ra03509c

rsc.li/rsc-advances

In this study, a newly-designed copper(II) complex of metformin and L-proline which was immobilized on $Fe_3O_4$ MNPs was developed. The structure of the catalyst platform was fully characterized using spectroscopic analyses. Moreover, the catalytic activity of [$Fe_3O_4$@Cu(II)(Met)(Pro-H)$_2$] was investigated in a one-pot synthesis of a variety of functionalized ethers in reasonable to excellent yields through Ullman reaction in an aqueous environment using various aryl halides, phenol, and $Cs_2CO_3$ and without using any external Cu-reducing agents. Notably, gentle catalytic conditions, quick reaction times, applicability, low cost, and preventing dangerous chemicals and solvents during synthesis and catalytic application are some of the superior properties of the [$Fe_3O_4$@Cu(II)(Met)(Pro-H)$_2$] complex. Furthermore, the catalyst can be reused for several runs (at least eight times) without remarkable loss in efficiency.

## 1. Introduction

Nowadays, supported heterogeneous catalysts have attracted a lot of interest due to their simplicity in product separation, which enables recycling, the versatility of the supports, which facilitates adaptability, and variable surface area due to changes in shape and composition, which boosts overall efficiency to achieve maximum yield.[1–5] A further benefit of the magnetic supports is their ease of mechanical separation.[2,6] As a result, the current research has focused on the use of magnetic nanocomposites for their better physical and mechanical qualities, as well as their economic and environmental benefits.[7,8] Due to their outstanding magnetic characteristics, high surface area and high catalytic activity, mixed metal oxide nanocomposites—especially metal-ferrites—are widely used in synthetic organic chemistry.[9–12]

Copper is often used in homo- and cross-coupling reactions that result in the creation of C–C, C–N, and C–O bonds.[13–16] In order to successfully produce diaryl ethers, it is the common procedure to make use of supported palladium and copper catalysts.[17] This cross-coupling reaction involves the use of aryl halides and phenols. Regarding the use of aryl halide-phenol cross-coupling technique, highly functionalized diaryl ethers may be produced in a more straightforward and time-efficient manner.[17–19] Diaryl ethers have a variety of applications, *i.e.* in producing novel materials with improved functionalities, synthesis, and creating new medications.[20–22] The Ullmann reaction has been put to use over the course of many years in the process of direct synthesis of aryl–heteroatom bonds originating from aryl halides.[17,23,24] This is because the Ullmann reaction is very effective and produces just a limited amount of unwanted byproducts. The Ullmann reaction, which is used in the synthesis of the functionalized diaryl ethers, necessitates the presence of severe reaction conditions, an extended reaction duration, and an inert environment.

Numerous procedures using various reagents have been described so far for the Ullmann synthesis of diaryl ethers.[25–27] In this sense, homogeneous copper-mediated methods have attracted interesting attention.[28–30] Heretofore, various reducing agents have been utilized as an electron source to activate the Cu species.[31–33] The major downsides of utilizing these chemicals are their low selectivity for desired products, production of unwanted and ecologically harmful by-products, need for stoichiometric concentration of reagents, the length of reaction durations, catalyst disposable and their reactivity with other functional groups.

[a]*Department of Pharmaceutical Chemistry, College of Pharmacy, University of Basrah, Iraq*
[b]*Department of Ecology Science, College of Science, Kufa University, Iraq*
[c]*Department of Pharmacy, Al-Manara College for Medical Sciences, Iraq*
[d]*Department of Chemical Engineering and Petroleum Industries, Al-Mustaqbal University College, 51001 Hilla, Babylon, Iraq*
[e]*Department of Computer Engineering Technology, Al Kitab University, Altun Kopru, Kirkuk 00964, Iraq*
[f]*Department of Medical Laboratories Technology, National University of Science and Technology, Dhi Qar, Iraq*
[g]*College of Dentistry, Uruk University, Baghdad, Iraq*
[h]*Chemistry Department, College of Science, University of Baghdad, Baghdad, Iraq. E-mail: haider.200690@gmail.com; h_r200690@yahoo.com*

† Electronic supplementary information (ESI) available. See DOI: https://doi.org/10.1039/d3ra03509c

Metformin consists of a 1,1-dimethyl-biguanide structure, in which two guanide molecules are bonded together, with a mode of action and application comparable to other biguanides.[34] The intermolecular hydrogen bonding, conjugation system and arrangement of C=NH groups and their N–C=NH ↔ R–N=C–NH resonance forms – consisting of anomeric effects – increase the electron-donating ability of NH groups and turn it into an attractive ligand. On the other hand, the presence of an $NH_2$ group at the end of the molecule chain gives it a special ability for further functionalization.[35–37] Metformin was previously used as a biguanide ligand in copper-catalyzed Ullmann-type C–N and C–O cross-couplings that show its ability in these types of reactions.[38] To address the above-mentioned deficiencies, we focus on the immobilization of metformin on the nanomagnetic $Fe_3O_4$ MNPs and its complexation with copper nitrate trihydrate and L-proline to generate the desired biguanide–copper catalyst for Ullmann-type cross-coupling of aryl halides with phenol – which results in generating the diaryl ethers under green conditions.

## 2. Experimental

### 2.1. Typical procedure for the synthesis of $[Fe_3O_4@Cu(II)(Met)(Pro\text{-}H)_2]$ MNPs

The initial step was to synthesize $Fe_3O_4$ MNPs using the chemical co-precipitation technique[39] and, then, a layer of alkyl chloride functionalities was placed around their surface using the CPTMS linker as mentioned in scientific literature.[40] In the next step, 1 g of $Fe_3O_4$@CPTMS was dispersed in DMSO containing 5 mmol of NaI (0.745 g) for 30 min and, then, 5 mmol of metformin (0.646 g) was added to the reaction mixture and stirred under reflux conditions for 48 hours. After the mixture was cooled, the synthesized $Fe_3O_4$@metformin MNPs were accumulated using an external magnet, washed with water and ethanol and, finally, dried at 80 °C. Eventually, 1 g of $Fe_3O_4$@-metformin MNPs was dispersed in 100 mL of ethanol and, then, it was treated with $Cu(NO_3)_2 \cdot 3H_2O$ (0.241 g, 1 mmol) and proline (0.230 g, 2 mmol) and stirred under reflux conditions for 24 h. The obtained $[Fe_3O_4@Cu(II)(Met)(Pro\text{-}H)_2]$ complex was accumulated applying an external magnet, washed using water and, finally, dried at 80 °C.

### 2.2. General procedure for the preparation of 2,4-diarylquinoline derivatives in the presence of $[Fe_3O_4@Cu(II)(Met)(Pro\text{-}H)_2]$

A mixture of phenol (1 mmol), aryl halide (1 mmol), $Cs_2CO_3$ (1.5 mmol) and $[Fe_3O_4@Cu(II)(Met)(Pro\text{-}H)_2]$ (8 mg) was stirred in water (2 mL) for the appropriate time at reflux conditions. After reaction completion, it was monitored using TLC. Furthermore, the catalyst was collected *via* magnetic decantation and, then, the produced organic product was extracted using ethyl acetate. Subsequently, it was dried using anhydrous sodium sulfate and, then, purified applying column chromatography.

## 3. Results and discussion

### 3.1. Characterization of the catalyst

It is in Scheme 1 that preparation of the catalyst is depicted. The following approaches were used to extensively characterize the as-prepared catalyst.

**3.1.1. FT-IR spectroscopy.** In order to explore the synthesis of catalytic support and stabilization of diverse functional groups; including, linker, ligand and formation of catalytic complex on its surface, FTIR analysis was performed on different synthesis stages. As depicted in Fig. 1, the $Fe_3O_4$, $Fe_3O_4$@CPTMS and $Fe_3O_4$@Met FT-IR spectra perfectly match with the earlier reports on the fingerprint of these samples.[41,42] The peaks appearing at 580 $cm^{-1}$ and 630 $cm^{-1}$ are attributed to characteristic stretching vibration mode of metal–oxygen (Fe–O) bonds.[43] Moreover, the faint peak at 810 $cm^{-1}$ and the sharp and broad absorption peaks at around 960 $cm^{-1}$ to ~1200 $cm^{-1}$ are attributed to symmetric and asymmetric Si–O–Si bond stretches, respectively.[44] The bands from 1954 $cm^{-1}$ to 1988 $cm^{-1}$ are due to the C–H stretching vibrations of the $CH_2$ groups of the CPTMS linker.[40] Regarding $Fe_3O_4$@Met MNPs, C–Cl peak was not observed in the spectra because of its removal

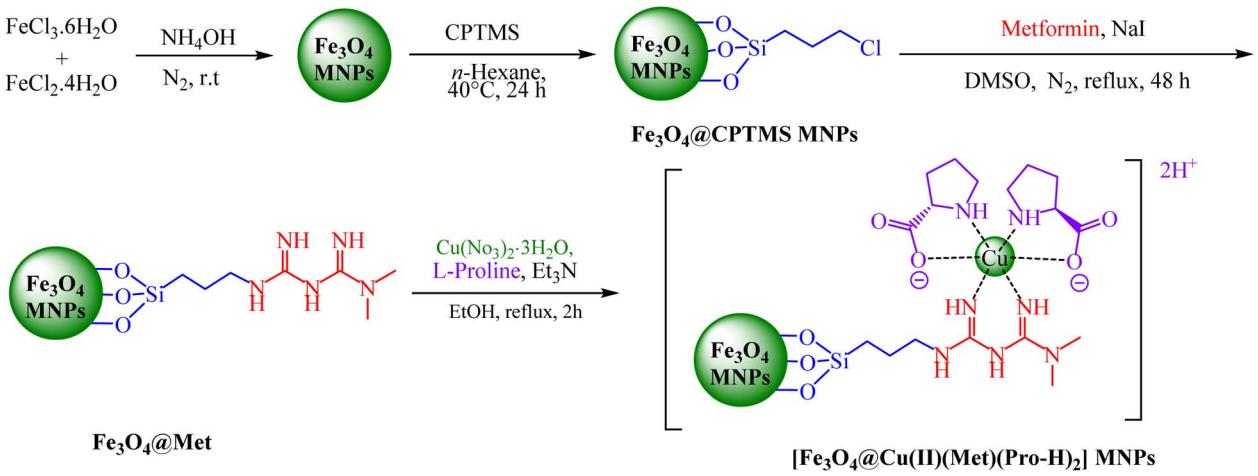


Scheme 1 Synthesis of $[Fe_3O_4@Cu(II)(Met)(Pro\text{-}H)_2]$ MNPs.

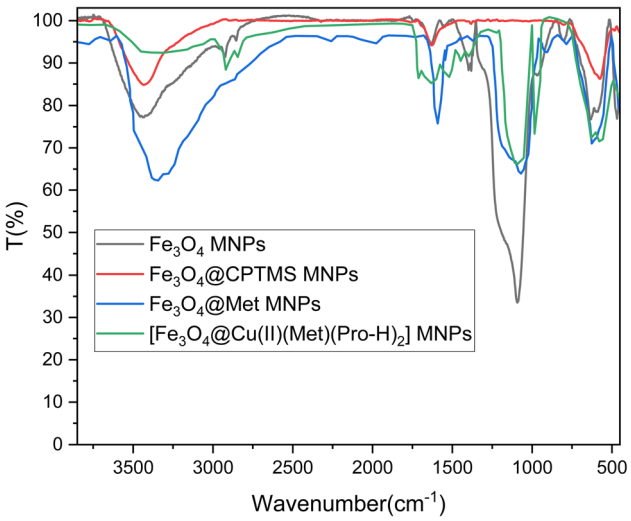


Fig. 1 FTIR of (black curve) $Fe_3O_4$, (red curve)) $Fe_3O_4$@CPTMS, (blue curve) $Fe_3O_4$@Met and (green curve) [$Fe_3O_4$@Cu(II)(Met)(Pro-H)$_2$] MNPs.

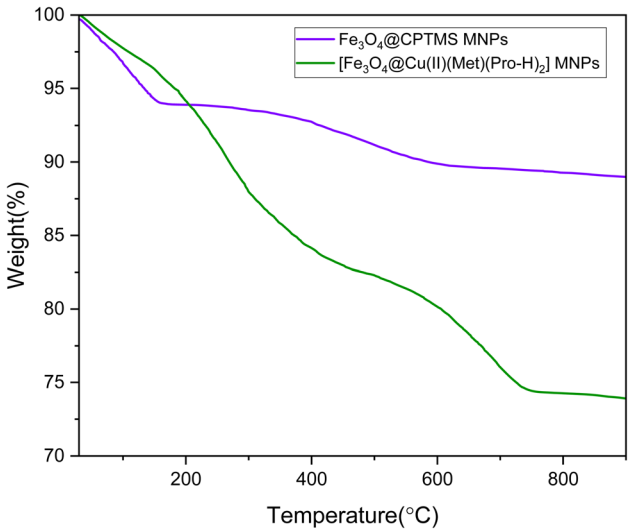


Fig. 3 TGA analysis of $Fe_3O_4$@CPTMS and [$Fe_3O_4$@Cu$^{(II)}$(Met)(Pro-H)$_2$] MNPs.

during $S_N2$ nucleophilic substitution reaction. Furthermore, the stretching vibrations of C=N and C–N bands can be identified due to the presence of strong peaks in the band at around 1702 and 1636 $cm^{-1}$, that confirms the hybridization of metformin groups with the surface of modified nanoparticles.[45] Considering the FT-IR spectrum of [$Fe_3O_4$@Cu(II)(Met)(Pro-H)$_2$], the aberrance of C=O bands in addition to the shift on C=N band can clearly confirm the complexation of Cu with L-proline and the heterogenized metformin moieties and also the generation of [Cu(II)(Met)(Pro-H)$_2$] complex on the surface of $Fe_3O_4$ MNPs.[46]

**3.1.2. P-XRD characterization.** The crystalline structure of [$Fe_3O_4$@Cu(II)(Met)(Pro-H)$_2$] complex was assessed using XRD measurements (Fig. 2). The XRD pattern shows a high degree of crystallization and characteristic peaks of $Fe_3O_4$ at $2\theta = 30.23°$, 35.60°, 43.50°, 54.01°, 57.49°, 62.86°, 71.48°, and 74.27°. Furthermore, due to the addition of CPTMS linker and its polymerization around the surface, $SiO_2$ amorphous phase peaks can be observed at around $2\theta = 17$–29°, demonstrating successful hybridization of inorganic support and organic phases in nanocomposites. Furthermore, the average particle size of the [$Fe_3O_4$@Cu(II)(Met)(Pro-H)$_2$] MNPs turned out to be 23.57 nm using the Scherer equation.

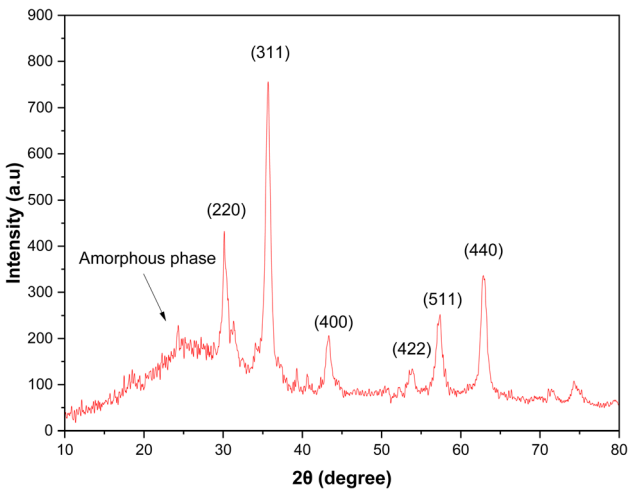


Fig. 2 XRD pattern of [$Fe_3O_4$@Cu(II)(Met)(Pro-H)$_2$] MNPs.

**3.1.3. Thermogravimetric analysis.** To examine the stability of the produced catalyst, thermogravimetric analysis (TGA) was performed (Fig. 3). Moreover, it is worth mentioning that the TGA curves reveal three phases of deterioration. At the first step, a typical weight loss of 6% is observed in the composites (happened before 200 °C) which is due to the removal of the moisture. Furthermore, the second step starts at above 230 °C. Regarding $Fe_3O_4$@CPTMS (about 5%), this step is attributed to CPTMS linker removal through the thermal decomposition to produce $CO_2$ and water gases. Considering $Fe_3O_4$@Cu(II)(Met)(Pro-H)$_2$, the observed increment (about 20%) at the weight loss is attributed to the decomposition of the immobilized metformin and L-proline organic moieties in [Cu(II)(Met)(Pro-H)$_2$] complex (Fig. 3). Notably, these findings attest to the effective synthesis of the intended catalyst. Consistent with these results, the [$Fe_3O_4$@Cu(II)(Met)(Pro-H)$_2$] is stable before 200 °C and can be used in various organic transformations.

**3.1.4. Elemental analysis.** Regarding EDX analysis, the elemental composition of [$Fe_3O_4$@Cu(II)(Met)(Pro-H)$_2$] MNPs was assessed, verifying the presence of the Fe, O, Si, C, N, and Cu components. Significantly, the findings are in good agreement with the expected composition of the desired catalytic support and its surface functionalities (Fig. 4). As shown in Fig. 4, the absence of Cl and presence of copper affirm the successful immobilization of metformin and also the construction of the final complex, respectively.

**3.1.5. Elemental mapping analysis.** Elemental mapping studies were used to analyze how the above-mentioned elements were distributed, the results of which demonstrate that the components of the produced structure – including iron, oxygen,

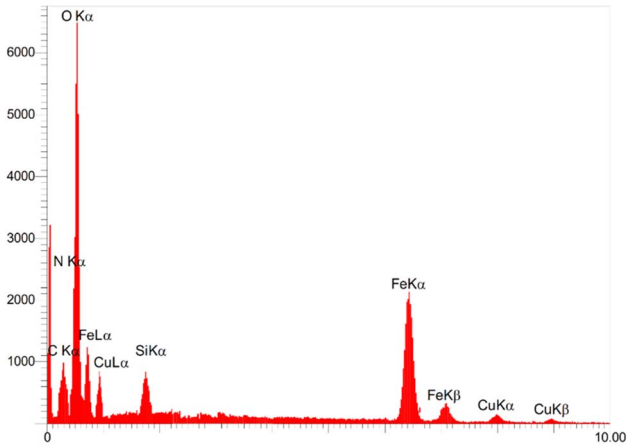


Fig. 4 EDX analysis of $[Fe_3O_4@Cu^{(II)}(Met)(Pro\text{-}H)_2]$ complex.

silica, carbon, nitrogen, and copper – were uniformly distributed on the catalyst surface (Fig. 5). Additionally, $[Fe_3O_4@Cu^{(II)}(Met)(Pro\text{-}H)_2]$ MNPs examination, applying inductively coupled plasma atomic emission spectroscopy (ICP-AES), revealed the presence of 1.27 mmol of Cu per 1 gram of the sample.

**3.1.6. SEM analysis.** Fig. 6 illustrates SEM image of $[Fe_3O_4@Cu(II)(Met)(Pro\text{-}H)_2]$ MNPs, in which it can be seen that the surface of the bar $Fe_3O_4$ MNPs is potentially covered *via* a mixture of the linker and catalytic complex composites, confirming an even functionalization of the catalyst nano-surface. Regarding the higher-magnification photographs at nano-scale, it can be seen that the surface of the coated particles seemed comparatively smooth and the approximately spherical particles are formed in average size of 18–28 nm. Despite this finding, the characteristics of spinel ferrite support persisted inside the structure, preserving a large specific surface area for high efficiency in catalysis applications.

**3.1.7. TEM analysis.** TEM analysis was carried out to get additional information and in-depth morphological and structural information of $[Fe_3O_4@Cu(II)(Met)(Pro\text{-}H)_2]$ MNPs sample (Fig. 7). TEM image describes that the particles were formed in average size of 18–27 nm with a spherical structure, in which the catalytic complex together with catalyst support and $[Cu(II)(Met)(Pro\text{-}H)_2]$ shell – that covers spinel iron particles – have a thickness of around 5–8 nm. The HR-TEM results also show that the as-prepared $[Fe_3O_4@Cu^{(II)}(Met)(Pro\text{-}H)_2]$ MNPs have an excellent single-crystal structure. Herein, it is worth noting that the particle dispersion is dense and the crystal superposition is shown by the dark color patches. This effect predicts that there will be a significant particle interaction and that excellent stability during the catalysis process will result from that contact.

**3.1.8. Magnetic properties.** The magnetic power of $[Fe_3O_4@Cu(II)(Met)(Pro\text{-}H)_2]$ nanoparticles was determined using VSM analysis. The saturation magnetization of the catalyst (57.03 emu $g^{-1}$) is, as predicted, much lower than that of $Fe_3O_4$ nanoparticles (98 emu $g^{-1}$).[47,48] The addition of CPTMS linker, metformin ligand and the final $[Cu(II)(Met)(Pro\text{-}H)_2]$ complex to the surface of iron nanoparticles causes this decrease. However, the prepared nano-catalyst retains significant magnetic characteristics and can be readily isolated from the reaction mixture using an external magnet (Fig. 8).

### 3.2. Catalytic properties of $[Fe_3O_4@Cu^{(II)}(Met)(Pro\text{-}H)_2]$ complex

**3.2.1. Optimization of reaction parameters.** The $[Fe_3O_4@Cu^{(II)}(Met)(Pro\text{-}H)_2]$ complex was successfully made and

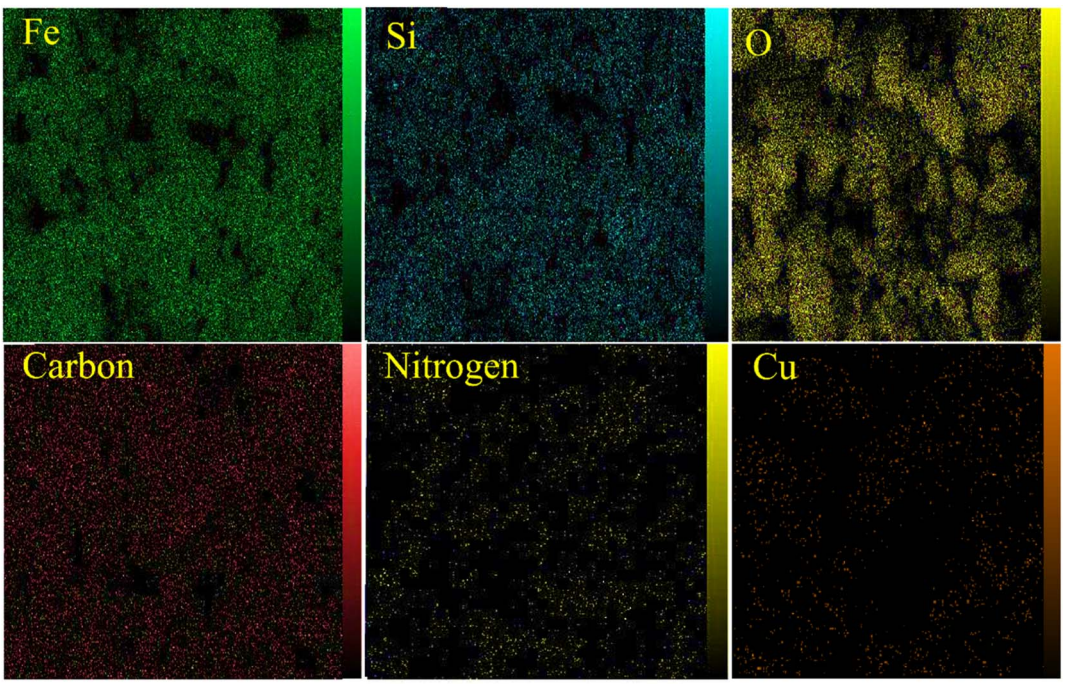


Fig. 5 EDX-mapping images of $[Fe_3O_4@Cu^{(II)}(Met)(Pro\text{-}H)_2]$ complex.

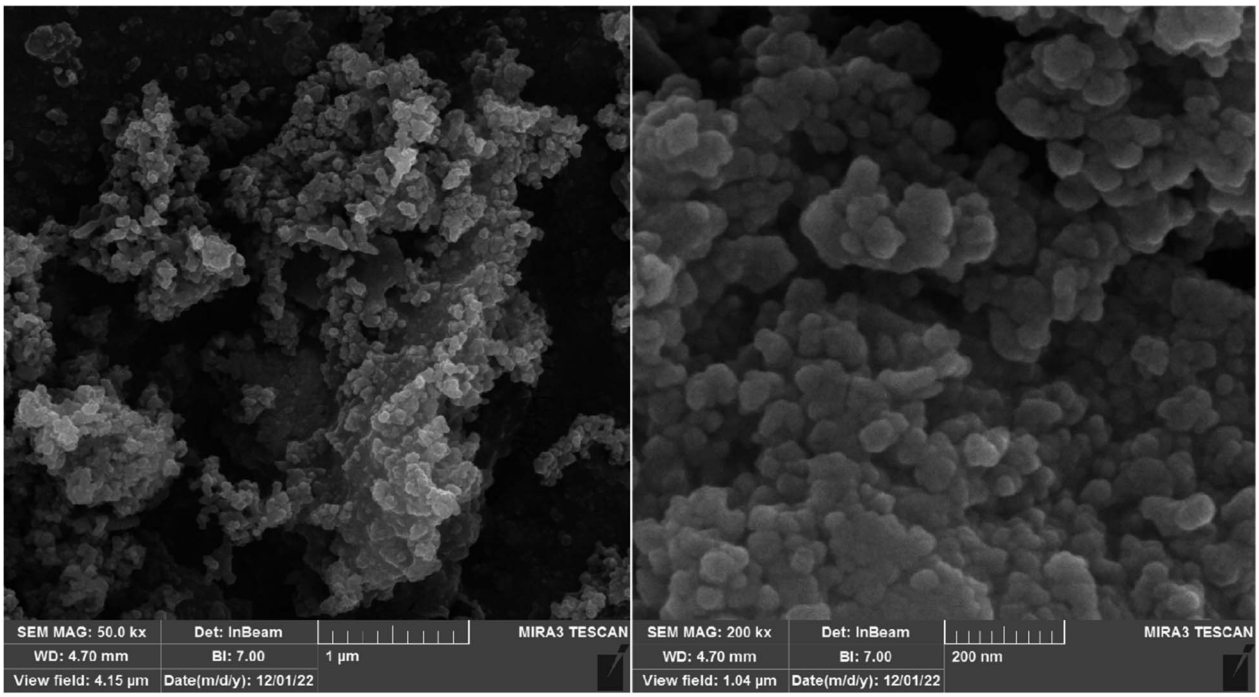


Fig. 6 SEM images of $[Fe_3O_4@Cu^{(II)}(Met)(Pro\text{-}H)_2]$ complex.

characterized. Afterwards, its catalytic effectiveness in the Ullmann synthesis of diaryl ethers was evaluated. This choice was made with the presumption that, under basic conditions, $Cu^{(II)}$ complex seems to provide a formidable weapon for the C–X bond insertion reaction to the substituted aryl halides and its cross-coupling reaction with nucleophiles – *i.e.* deprotonated

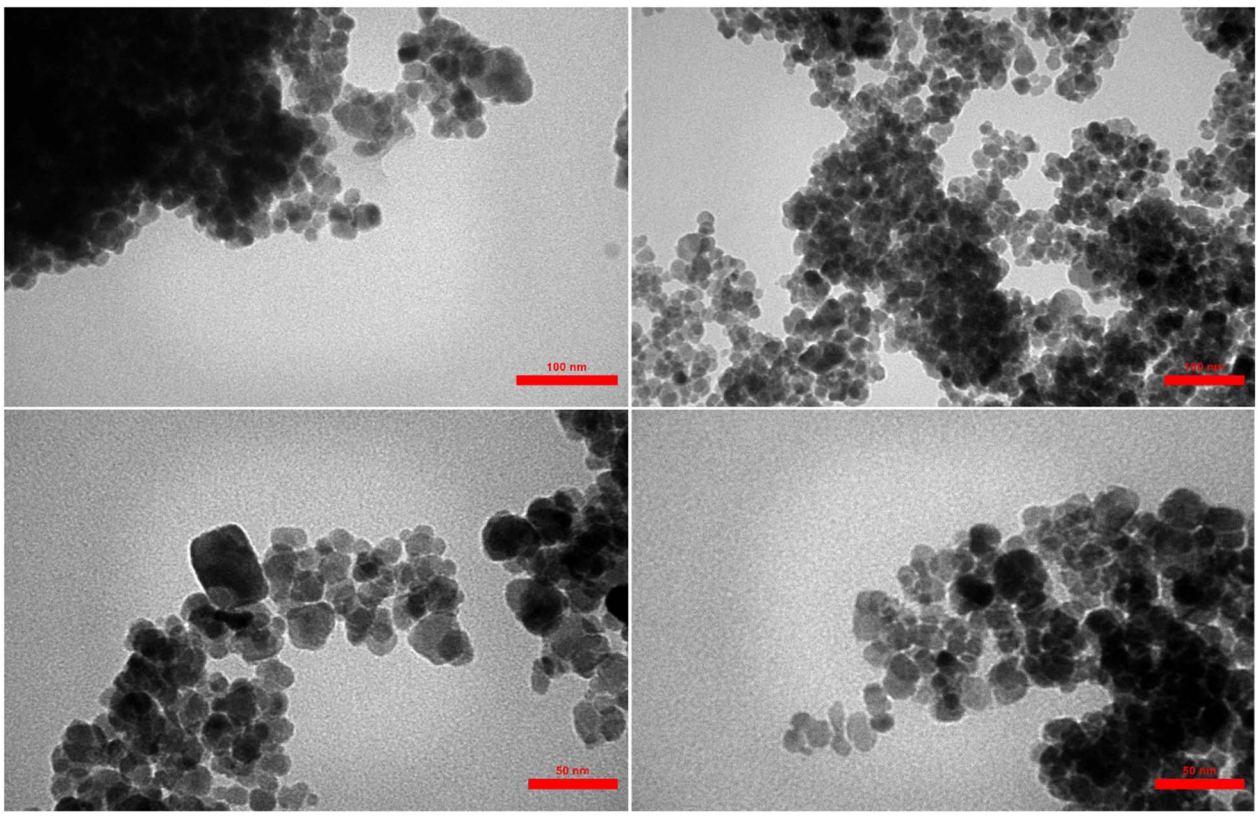


Fig. 7 TEM images of $[Fe_3O_4@Cu^{(II)}(Met)(Pro\text{-}H)_2]$ complex.

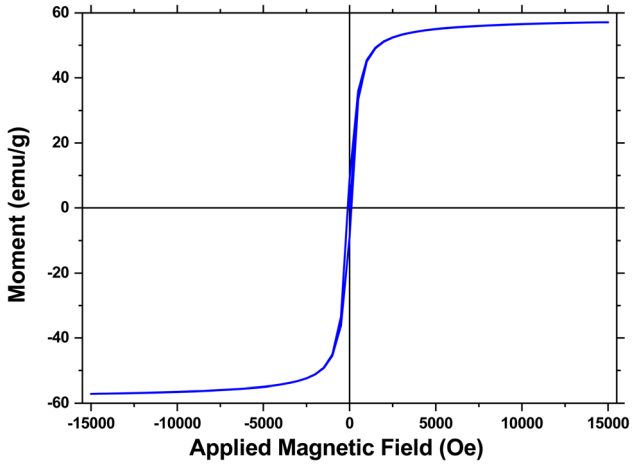


Fig. 8 VSM analysis of $[Fe_3O_4@Cu^{(II)}(Met)(Pro\text{-}H)_2]$ complex.

phenol. In order to achieve the Ullmann synthesis of diaryl ethers, the reaction of iodobenzene (1 mmol), phenol (1 mmol), and $K_2CO_3$ (1.5 mmol) – in presence of $[Fe_3O_4@Cu^{(II)}(Met)(Pro\text{-}H)_2]$ in 2 mL of water – was taken into consideration as the model reaction. In addition, various tests were designed to determine the optimal conditions for this organic transformation. In the first step, the amount of the catalyst was varied from 0 to 10 mg, and the results of the study showed that the yield increased in direct proportion to the amount of catalyst used (entries 1–6, Table 1). Although the highest yield was obtained when 8 mg of $[Fe_3O_4@Cu^{(II)}(Met)(Pro\text{-}H)_2]$ was employed, no significant increment was occurred as compared to the run using 10 mg of the catalytic complex under the same conditions (entry 5 *vs.* entry 6, Table 1). As a result, 80 mg of the $[Fe_3O_4@Cu^{(II)}(Met)(Pro\text{-}H)_2]$ was chosen as the optimal catalyst amount for future optimization.

The influence of the solvent on the model reaction was then examined (entries 7–12, Table 1). Accordingly, the good yield in water prompted the use of green solvents. Thus, a variety of sustainable mediums was investigated to provide a high yield of the required product. Initially, we performed the reaction in nonpolar solvents; but no substantial yield was detected (entries 7–9, Table 1). Furthermore, polar solvents such as PEG-400, EtOH and MeOH failed to produce a higher yield of C–O cross-coupling product in comparison to water (entries 8–12 *vs.* 6, Table 1). Significantly, considering reactions that occur on water, the hydrophobic nature of the reactants causes them to come closer together, leading to an increase in reaction rates.

Table 1 Optimization of the Ullmann synthesis of diphenyl ethers over the catalysis of $[Fe_3O_4@Cu^{(II)}(Met)(Pro\text{-}H)_2]$ complex under different conditions

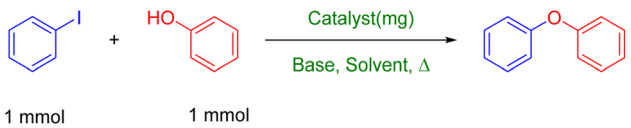


| Entry | Amount of catalyst (mg) | Base type | Solvent | Temperature (°C) | Time (h) | Yield[a,b] (%) |
|---|---|---|---|---|---|---|
| 1 | — | $K_2CO_3$ | Water | Reflux | 5 | NR |
| 2 | 2 | $K_2CO_3$ | Water | Reflux | 1 | 49 |
| 3 | 4 | $K_2CO_3$ | Water | Reflux | 1 | 78 |
| 4 | 6 | $K_2CO_3$ | Water | Reflux | 1 | 90 |
| 5 | 8 | $K_2CO_3$ | Water | Reflux | 1 | 93 |
| 6 | 10 | $K_2CO_3$ | Water | Reflux | 1 | 93 |
| 7 | 8 | $K_2CO_3$ | *n*-Hexane | Reflux | 1 | NR |
| 8 | 8 | $K_2CO_3$ | Cyclohexane | Reflux | 1 | NR |
| 9 | 8 | $K_2CO_3$ | Toluene | 100 | 1 | Trace |
| 10 | 8 | $K_2CO_3$ | PEG-400 | 100 | 1 | 88 |
| 11 | 8 | $K_2CO_3$ | EtOH | Reflux | 1 | 84 |
| 12 | 8 | $K_2CO_3$ | MeOH | Reflux | 1 | 87 |
| 13 | 8 | — | Water | Reflux | 1 | Trace |
| 14 | 8 | KOH | Water | Reflux | 1 | 23 |
| 15 | 8 | NaOH | Water | Reflux | 1 | 27 |
| 16 | 8 | $Na_2CO_3$ | Water | Reflux | 1 | 96 |
| 17 | 8 | $Cs_2CO_3$ | Water | Reflux | 1 | 98 |
| 18 | 8 | $Et_3N$ | Water | Reflux | 1 | 47 |
| 19 | 8 | Pyridine | Water | Reflux | 1 | 35 |
| 20 | 8 | $Cs_2CO_3$ | Water | 80 | 1 | 84 |
| 21 | 8 | $Cs_2CO_3$ | Water | 60 | 1 | 42 |
| 22 | 8 | $Cs_2CO_3$ | Water | 40 | 1 | 31 |
| 23 | 8 | $Cs_2CO_3$ | Water | r.t. | 3 | Trace |

[a] Reaction conditions: iodobenzene (1 mmol), phenol (1 mmol) and base (1.5 mmol) catalyst (mg) and solvent (2 mL). [b] Isolated yields.

Table 2 The Ullmann synthesis of diaryl ethers over the catalysis of $[Fe_3O_4@Cu^{(II)}(Met)(Pro\text{-}H)_2]$ complex in water

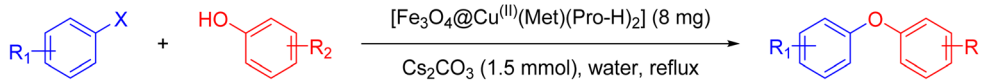


| Entry | Aryl halide | Phenol | Product | Time (min) | Yield[a,b] (%) | Melting point | |
|---|---|---|---|---|---|---|---|
| | | | | | | Found | Ref. |
| 1 |  | 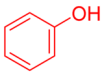 | 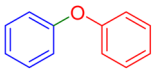 | 60 | 98 | Oil | Oil[53] |
| 2 | 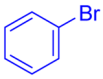 | 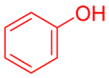 | 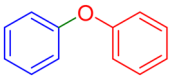 | 180 | 96 | Oil | Oil[53] |
| 3 |  | 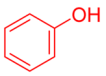 | 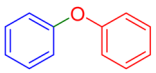 | 480 | 89 | Oil | Oil[53] |
| 4 | 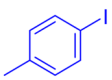 | 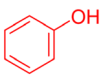 | 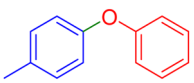 | 95 | 93 | Oil | Oil[53] |
| 5 | 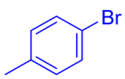 | 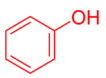 | 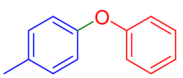 | 240 | 90 | Oil | Oil[53] |
| 6 | 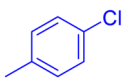 | 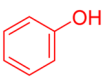 | 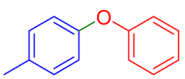 | 380 | 84 | Oil | Oil[53] |
| 7 | 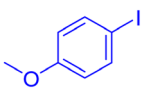 | 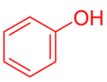 | 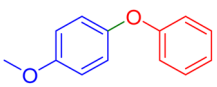 | 245 | 86 | Oil | Oil[53] |
| 8 | 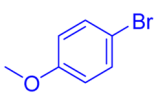 | 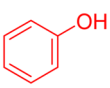 | 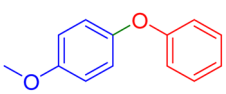 | 480 | 81 | Oil | Oil[53] |
| 9 | 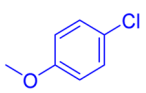 | 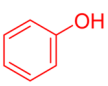 | 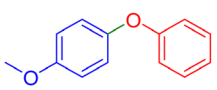 | 720 | 74 | Oil | Oil[53] |
| 10 | 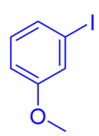 | 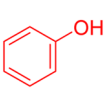 | 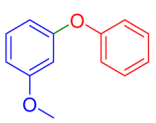 | 120 | 87 | Oil | Oil[53] |
| 11 | 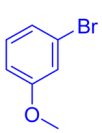 | 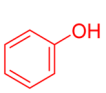 | 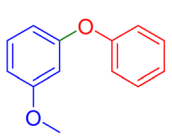 | 185 | 82 | Oil | Oil[53] |
| 12 | 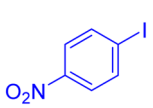 | 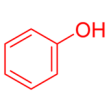 | 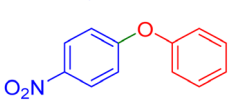 | 35 | 95 | 55–57 | 57–59 (ref. 53) |
| 13 | 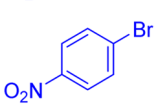 | 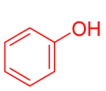 | 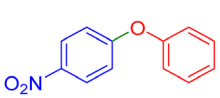 | 60 | 87 | 55–57 | 57–59 (ref. 53) |
| 14 |  |  |  | 85 | 97 | 55–57 | 57–59 (ref. 53) |

Table 2 (*Contd.*)

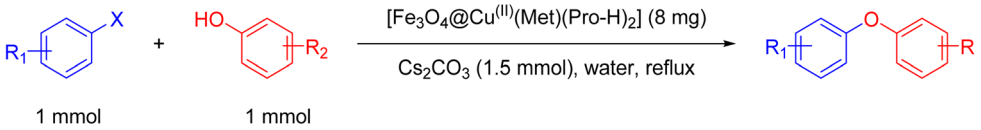


| Entry | Aryl halide | Phenol | Product | Time (min) | Yield[a,b] (%) | Melting point Found | Melting point Ref. |
|---|---|---|---|---|---|---|---|
| 15 | 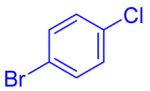 | 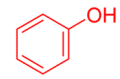 | 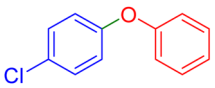 | 35 | 74 | Oil | Oil[53] |
| 16 |  | 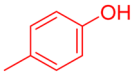 | 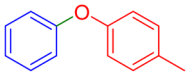 | 100 | 93 | Oil | Oil[53] |
| 17 |  | 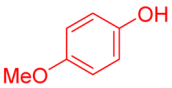 | 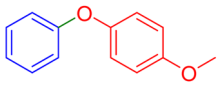 | 300 | 88 | Oil | Oil[53] |
| 18 |  | 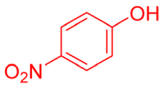 | 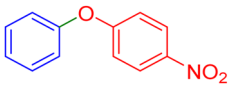 | 95 | 96 | 56–58 | 57–59 (ref. 53) |

[a] Conditions: aryl halide (1 mmol), phenol (1 mmol), $Cs_2CO_3$ (1.3 mmol) and $[Fe_3O_4@Cu^{(II)}(Met)(Pro\text{-}H)_2]$ (8 mg) in reflux of water (2 mL). [b] Isolated yields.

Additionally, the hydrogen bonding between organic compounds and water at the interface can activate the reactants and sometimes stabilize the transition states. Therefore, water can serve as both a solvent and a catalyst in these reactions.[49–52] Fortunately, water was identified to be the suitable solvent, due to the act that it produced a high yield of the target product in a low reaction temperature and minimized the release of dangerous chemicals into the environment (entry 6, Table 1).

Afterwards, numerous inorganic and organic bases were screened as part of the optimization research (entries 14–19, Table 1). In the absence of a base, a really low yield of the diaryl ether product was achieved (entry 13, Table 1). Strong bases, including KOH and NaOH produced modest yields (entries 14–15, Table 1). Considering a variety of bases, $Cs_2CO_3$ was identified to be an appropriate base for the high yield synthesis of the target product (entry 18, Table 1).

Further efforts (entries 20–23, Table 1) revealed that the temperature was more effective on the reaction efficiency than any other parameter. At room temperature, the Ullmann synthesis of diaryl ethers required a longer reaction time, resulting in a considerably decreased product. Considering the product yield, the optimal parameters of the present protocol are 8 mg of catalyst and 1.5 equivalents of $Cs_2CO_3$ in an aqueous medium at reflux conditions (entry 17, Table 1).

**3.2.2. Reaction scope.** Therefore, the generality and practical versatility of $[Fe_3O_4@Cu^{(II)}(Met)(Pro\text{-}H)_2]$ complex-catalyzed Ullmann synthesis of diaryl ethers under the optimized conditions were explored using various combinations of the substituted aryl halide and phenol substrates under standard conditions (Table 2). In most cases, highly functionalized diaryl ether adducts were synthesized from the reaction of different substituted aryl halides (I, Br and Cl) and phenol in good to outstanding yields with no by-products. The catalyst indicated unique performance for aromatic halides including electron-donating and electron-withdrawing groups. The reaction proceeded easily for highly functional aryl halides and led the synthesis of highly substituted diaryl ethers in good yields. According to the results, aryl iodides are much more reactive than aryl bromides and chlorides, respectively. Additionally, it is worth mentioning that phenols bearing different functional groups splendidly reacted under the optimal conditions. Moreover, we believe that the absence of homo-coupling products further supports the selectivity and efficiency of our developed method. Finally, a gram-scale experiment was performed on the model reaction and, accordingly, the corresponding diphenyl ether was successfully isolated with 96% of yield, confirming the scalability of this procedure.

**3.2.3. Reaction mechanism.** Based on earlier studies,[54] Fig. 3 shows a probable mechanism for the reductive Ullmann C–O cross-coupling reaction. Initially, Ar–O–Cu species are formed through the base-assisted deporotonation of phenol and its nucleophilic substitution to the Cu complex. In the next step, the copper complex undergoes oxidative addition into the aryl bond, resulting in the formation of intermediate (b). In the next step, the base-assisted displacement of the halogen atom leads to the formation of intermediate (c). Finally, the reductive

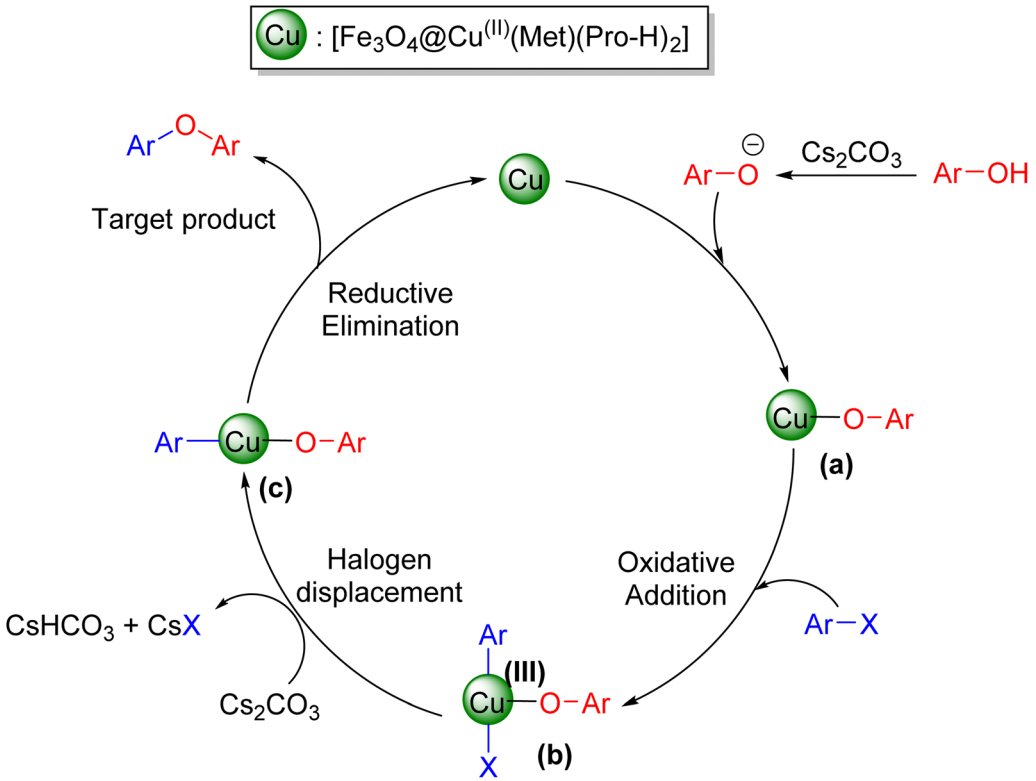


Scheme 2 The proposed mechanism for the Ullmann synthesis of diaryl ethers over $[Fe_3O_4@Cu^{(II)}(Met)(Pro\text{-}H)_2]$ catalyst.

elimination produces the required diaryl ether product and regenerates catalytic Cu species (Scheme 2).

### 3.3. Cycling stability

One of the most notable characteristics of environmentally friendly catalysts is their capacity to be recycled. In fact, the reusability of a new catalyst should be checked in order to understand its cycling stability and operational applicability. In this regard, a research on the reusability of the synthesized $[Fe_3O_4@Cu^{(II)}(Met)(Pro\text{-}H)_2]$ complex was carried out. After the reaction was finished, an external magnet was used to separate the $[Fe_3O_4@Cu^{(II)}(Met)(Pro\text{-}H)_2]$ catalytic complex from the reaction medium. Afterwards, the nanocomposite was washed using water, acetone, and ethanol. Eventually, the newly acquired catalyst was used in the subsequent reaction cycles. It is intriguing to note that the recovered $[Fe_3O_4@Cu^{(II)}(Met)(Pro\text{-}H)_2]$ complex could maintain its catalytic activity with very little loss throughout the course of eight consecutive reaction cycles, as shown in Fig. 9.

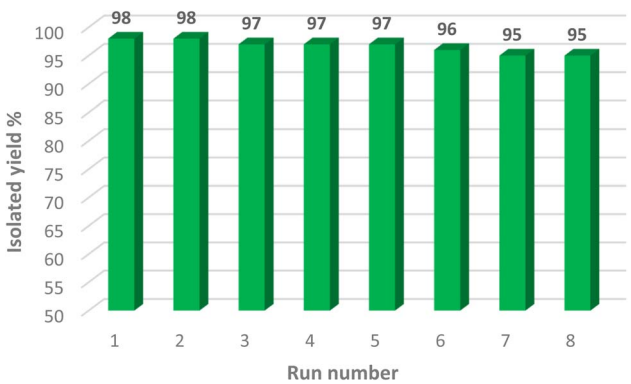


Fig. 9 Reusability of $[Fe_3O_4@Cu^{(II)}(Met)(Pro\text{-}H)_2]$ MNPs.

**3.3.1. Hot-filtration and leaching test.** In order to evaluate the $[Fe_3O_4@Cu^{(II)}(Met)(Pro\text{-}H)_2]$ MNPs heterogeneity, hot filtration test was carried out. After 10–20% of conversion, $[Fe_3O_4@Cu^{(II)}(Met)(Pro\text{-}H)_2]$ MNPs were completely withdrawn from the reaction mixture so as to reduce the amount of leached copper that would be reabsorbed onto the surface of the catalyst. Moreover, the filtrate was reintroduced into the oil bath and was allowed to proceed for the remaining time of its progress. Following the completion of the reaction, the filtrate was collected in order to conduct an analysis using ICP-AES to quantify the content of leached copper. Significantly, copper was not detected in the filtrate in any appreciable concentrations at all. Furthermore, the rate of conversion in the collected filtrates did not rise any further after the separation of the catalyst. The results of the hot filtration and leaching tests demonstrate that $[Fe_3O_4@Cu^{(II)}(Met)(Pro\text{-}H)_2]$ complex performs an effective catalytic function in the successful synthesis of the respective target molecules without causing any leaching to occur in the reaction media. Based on these findings, it seems that the nanocatalyst had a heterogeneous composition.

**3.3.2. Comparison.** Table 3 presents the results of a comparison between the effectiveness of our method and that

Table 3 Comparison the efficiency of [$Fe_3O_4$@Cu(II)(Met)(Pro-H)$_2$] with existing catalysts

| Entry | Catalyst | Time (min) | Yield[a] (%) | Ref. |
|---|---|---|---|---|
| 1 | Cu-IS-AMBA | 180 | 97 | 55 |
| 2 | $Fe_3O_4$@AMCA-MIL53(Al)-$NH_2$-$Co^{II}$ | 360 | 95 | 56 |
| 3 | (1,4-$C_6H_4$)(GO-CPTMS@HPTPy-Pd-TPy)$_2$ | 24 h | 96 | 57 |
| 4 | Cu-IS-AMBA-MNPs | 180 | 97 | 55 |
| 5 | MWCNTs-Met/CuCl | 8 | 96 | 35 |
| 6 | CuI | 22 h | 95 | 19 |
| 7 | [$Fe_3O_4$@Cu(II)(Met)(Pro-H)$_2$] | 60 | 98 | This work |

[a] Isolated yields.

of other methods proposed for the preparation of diaryl ethers. Regarding the current method, [$Fe_3O_4$@Cu(II)(Met)(Pro-H)$_2$] complex produced higher yields while maintaining the same level of efficiency. On the contrary, the previously reported methodologies were mediated by costly catalysts. Notably, the use of this strategy as an alternative to the Ullmann C–O cross-coupling reactions is made possible by the combination of a low-cost complex and utilizing an environmentally friendly and recyclable solvent, which is water. Additionally, the suitability of this strategy is partly due to the fact that toxic materials are not applied and used.

## 4. Conclusion

Considering the L-proline–Cu-complex support, we were able to successfully show the use of a commonly accessible and environmentally friendly metformin-modified $Fe_3O_4$ MNPs platform in the course of this research. The [$Fe_3O_4$@Cu(II)(Met)(Pro-H)$_2$] complex was generated and evaluated – regarding its effectiveness in the Ullman reaction as a magnetic heterogeneous nanocatalyst that is environmentally friendly, efficient, stable, and reusable. The synthesis of diaryl ethers was successfully accomplished in reflux conditions of water as an environmentally friendly solvent. This approach resulted in high to exceptional yields of the respective ethers in a relatively short amount of time. The reported protocol offered notable features, *i.e.* using readily available commercial materials, applying relatively inexpensive raw materials, recyclability of the catalyst for at least four times, ease of catalyst separation from the reaction medium with the assistance of external magnets, short reaction times, good to decent yields with excellent selectivity, and gentle reaction conditions.

## Conflicts of interest

There are no conflicts to declare.

## References

1 M. Atarod, J. Safari and H. Tebyanian, *Synth. Commun.*, 2020, **50**, 1993–2006.
2 W. Sun, J. Zhu, M. Zhang, X. Meng, M. Chen, Y. Feng, X. Chen and Y. Ding, *Chin. J. Catal.*, 2022, **43**, 2273–2300.
3 F. Ghobakhloo, D. Azarifar, M. Mohammadi, H. Keypour and H. Zeynali, *Inorg. Chem.*, 2022, **61**, 4825–4841.
4 A. Nikseresht, R. Bagherinia, M. Mohammadi and R. Mehravar, *RSC Adv.*, 2023, **13**, 674–687.
5 H. Keypour, J. Kouhdareh, S. Alavinia, K. Rabiei, M. Mohammadi, A. Maryamabadi and S. Babaei, *J. Organomet. Chem.*, 2023, **989**, 122646.
6 V. B. Khajone, K. R. Balinge and P. R. Bhagat, *Catal. Lett.*, 2021, **151**, 1948–1960.
7 P. Salehpour and A. Abri, *Colloids Surf., B*, 2022, **220**, 112903.
8 F. Ghobakhloo, D. Azarifar and M. Mohammadi, *J. Phys. Chem. Solids*, 2023, **175**, 111222.
9 M. K. Bharti, S. Chalia, P. Thakur, S. N. Sridhara, A. Thakur and P. B. Sharma, *Environ. Chem. Lett.*, 2021, **19**, 3727–3746.
10 N. Thomas, D. D. Dionysiou and S. C. Pillai, *J. Hazard. Mater.*, 2021, **404**, 124082.
11 L. E. Caldeira, *Eng. Mater.*, 2022, 1–16.
12 M. A. C. Florez, G. F. Ribas, J. J. R. Rovira, A. M. M. García, S. A. S. da Mata, E. Rodríguez-Castellón and M. J. G. da Silva, *Metall. Mater. Trans. A*, 2022, **53**, 1276–1293.
13 K. Kunz, U. Scholz and D. Ganzer, *Synlett*, 2003, **2003**, 2428–2439.
14 F. Zhou and Q. Cai, *Beilstein J. Org. Chem.*, 2015, **11**, 2600–2615.
15 F. Cheng, T. Chen, Y.-Q. Huang, J.-W. Li, C. Zhou, X. Xiao and F.-E. Chen, *Org. Lett.*, 2022, **24**, 115–120.
16 Y. Liu and J. Wan, *Chem.–Asian J.*, 2012, **7**, 1488–1501.
17 H.-J. Cristau, P. P. Cellier, S. Hamada, J.-F. Spindler and M. Taillefer, *Org. Lett.*, 2004, **6**, 913–916.
18 S. Akkarasamiyo, S. Ruchirawat, P. Ploypradith and J. S. M. Samec, *Synthesis*, 2020, **52**, 645–659.
19 J. W. W. Chang, S. Chee, S. Mak, P. Buranaprasertsuk, W. Chavasiri and P. W. H. Chan, *Tetrahedron Lett.*, 2008, **49**, 2018–2022.
20 T. Chen, H. Xiong, J.-F. J.-F. Yang, X.-L. X.-L. Zhu, R.-Y. R.-Y. Qu and G.-F. G.-F. Yang, *J. Agric. Food Chem.*, 2020, **68**, 9839–9877.
21 K. Smith and D. Jones, *J. Chem. Soc., Perkin Trans. 1*, 1992, 407.
22 N. Jalalian, E. E. Ishikawa, L. F. Silva and B. Olofsson, *Org. Lett.*, 2011, **13**, 1552–1555.
23 Anuradha, S. Layek, B. Agrahari and D. D. Pathak, *ChemistrySelect*, 2017, **2**, 6865–6876.

24 M. L. Rahman, M. S. Sarjadi, C. J. Fui, S. Guerin, S. C. Pillai and S. M. Sarkar, *J. Cleaner Prod.*, 2023, **390**, 136015.
25 Z. Noorpoor and S. Tavangar, *J. Coord. Chem.*, 2021, **74**, 1651–1662.
26 R. M. Al-Zoubi, R. M. Altamimi, W. K. Al-Jammal, K. Q. Shawakfeh, M. S. Al-Zoubi, M. J. Ferguson, A. Zarour, A. Yassin and A. Al-Ansari, *Synth*, 2021, **53**, 2665–2675.
27 S. Tanaka and K. Maeyama, *Chem. Lett.*, 2023, **52**, 296–298.
28 C. J. Fui, M. S. Sarjadi, S. M. Sarkar and M. L. Rahman, *Catalysts*, 2020, **10**, 1103.
29 N. Kaur, *Synth. Commun.*, 2019, **49**, 879–916.
30 R. Akhtar, A. F. Zahoor, M. Irfan, T. H. Bokhari and A. ul Haq, *Chem. Pap.*, 2022, **76**, 7275–7293.
31 M. B. Gawande, A. Goswami, F.-X. Felpin, T. Asefa, X. Huang, R. Silva, X. Zou, R. Zboril and R. S. Varma, *Chem. Rev.*, 2016, **116**, 3722–3811.
32 A. Khan, A. Rashid, R. Younas and R. Chong, *Int. Nano Lett.*, 2016, **6**, 21–26.
33 M. Bollenbach, P. Wagner, P. G. V. Aquino, J. J. Bourguignon, F. Bihel, C. Salomé and M. Schmitt, *ChemSusChem*, 2016, **9**, 3244–3249.
34 M. T. da Trindade, A. C. Kogawa and H. R. N. Salgado, *Crit. Rev. Anal. Chem.*, 2018, **48**, 66–72.
35 E. Akhavan, S. Hemmati, M. Hekmati and H. Veisi, *New J. Chem.*, 2018, **42**, 2782–2789.
36 M. Nasrollahzadeh, Z. Nezafat, K. Pakzad and F. Ahmadpoor, *J. Organomet. Chem.*, 2021, **948**, 121915.
37 Z. S. Robatjazi, M. R. Naimi-Jamal and M. Tajbakhsh, *Sci. Rep.*, 2022, **12**, 4949.
38 R. Ghorbani-Vaghei, S. Hemmati and H. Veisi, *Tetrahedron Lett.*, 2013, **54**, 7095–7099.
39 B. Nammalwar, N. P. Muddala, R. Pitchimani and R. A. Bunce, *Molecules*, 2015, **20**, 22757–22766.
40 A. Jafari, S. Heydari, M. Ariannezhad, S. Ahmadi and D. Habibi, *Chem. Phys. Lett.*, 2022, **786**, 139195.
41 H. Yao, Y. Wang and M. K. Razi, *RSC Adv.*, 2021, **11**, 12614–12625.
42 A. Mazaheri and M. Bostanian, *Res. Chem. Intermed.*, 2020, **46**, 2327–2350.
43 N. Taheri, F. Heidarizadeh and A. Kiasat, *J. Magn. Magn. Mater.*, 2017, **428**, 481–487.
44 I. Dindarloo Inaloo, S. Majnooni, H. Eslahi and M. Esmaeilpour, *Appl. Organomet. Chem.*, 2020, **34**, e5662.
45 F. Hajizadeh, A. Amiri, B. Maleki and F. Mohammadi Zonoz, *Microchem. J.*, 2022, **175**, 107176.
46 G. K. Kharmawlong, R. Nongrum, B. Chhetri, J. W. S. Rani, N. Rahman, A. K. Yadav and R. Nongkhlaw, *Synth. Commun.*, 2019, **49**, 2683–2695.
47 M. Colombo, S. Carregal-Romero, M. F. Casula, L. Gutiérrez, M. P. Morales, I. B. Böhm, J. T. Heverhagen, D. Prosperi and W. J. Parak, *Chem. Soc. Rev.*, 2012, **41**, 4306.
48 M. D. Nguyen, H.-V. Tran, S. Xu and T. R. Lee, *Appl. Sci.*, 2021, **11**, 11301.
49 N. A. Harry, S. Radhika, M. Neetha and G. Anilkumar, *ChemistrySelect*, 2019, **4**, 12337–12355.
50 T. Kitanosono, K. Masuda, P. Xu and S. Kobayashi, *Chem. Rev.*, 2018, **118**, 679–746.
51 T. Kitanosono and S. Kobayashi, *Chem.–Eur. J.*, 2020, **26**, 9408–9429.
52 M. Cortes-Clerget, J. Yu, J. R. A. Kincaid, P. Walde, F. Gallou and B. H. Lipshutz, *Chem. Sci.*, 2021, **12**, 4237–4266.
53 A. Ghorbani-Choghamarani, Z. Seydyosefi and B. Tahmasbi, *Appl. Organomet. Chem.*, 2018, **32**, e4396.
54 R. Giri, A. Brusoe, K. Troshin, J. Y. Wang, M. Font and J. F. Hartwig, *J. Am. Chem. Soc.*, 2018, **140**, 793–806.
55 M. M. Khodaei, A. Alizadeh and M. Haghipour, *Res. Chem. Intermed.*, 2019, **45**, 2727–2747.
56 A. Mohammadinezhad and B. Akhlaghinia, *Catal. Lett.*, 2020, **150**, 332–352.
57 K. Bahrami and H. Targhan, *Appl. Organomet. Chem.*, 2019, **33**, e4842.